Journal of Magnetism and Magnetic Materials 475 (2019) 130–136

Contents lists available at ScienceDirect

Journal of Magnetism and Magnetic Materials

journal homepage: www.elsevier.com/locate/jmmm

Research articles

Enhanced magnetic properties of Zn doped Fe_3O_4 nano hollow spheres for better bio-medical applications

Priyanka Saha[a,*], Rupali Rakshit[b], Kalyan Mandal[a]

[a] Department of Condensed Matter Physics and Material Science, S. N. Bose National Centre for Basic Sciences, Block JD, Sector III, Salt Lake, Kolkata 700 106, India
[b] Nanoscience & Nanotechnology Center, The Institute of Scientific and Industrial Research, Osaka University, Mihogaoka 8-1, Ibaraki, Osaka 567-0047, Japan

ARTICLE INFO

Keywords:
Magnetic nanomaterials
Nano hollow spheres
Zn doped ferrite nanostructures
Enhanced magnetization
Reduced dipolar interaction

ABSTRACT

We synthesized $Zn_xFe_{3-x}O_4$ (x = 0.0, 0.1, 0.2, 0.3, 0.4, 1.0) nano-hollow spheres (NHSs), a promising functional magnetic material for bio-medical applications. Detailed temperature dependent magnetic studies indicate an increase in saturation magnetization (M_S) with Zn doping, attaining a maximum at x = 0.2 (M_S = 92.52 emu/g at room temperature), due to the replacement of antiferromagnetically coupled Fe_A^{3+} ion on the A site by Zn^{2+} and transformation of Fe_B^{2+} to Fe_B^{3+} on B site for maintaining the charge neutrality. The dynamic magnetic properties of the powdered $Zn_xFe_{3-x}O_4$ samples were investigated using frequency dependent real and imaginary parts of ac susceptibility. The data obtained by fitting Vogel Fulcher law indicates reduced dipolar interaction in our systems due to Zn doping. Applications of Fe_3O_4 nanostructures can be improved by doping Zn and making hollow spheres.

1. Introduction

Fe_3O_4 nanoparticles (NPs) are found to be potential candidates for many bio-medical applications, such as in targeted drug delivery, cancer therapy, imaging etc. and have been widely used in bio-medical field [1–4]. Though in all the applications high magnetization is required, it deteriorates significantly when size is reduced from bulk to nano, because of surface effects, where magnetic order is highly disturbed. Therefore enhancement of magnetization in Iron oxide nanostructures is a real challenge to the material scientists.

Doping Fe_3O_4 with divalent cation (Zn^{2+}, Co^{2+}, Mn^{2+}, Mg^{2+}, Ni^{2+} etc.) is an effective method to enhance magnetic properties [5–9]. Nano ferrites (MFe_2O_4) have aroused much attention in nanotechnology, bio-electronics, spintronics and bio-sensors [10–14] because of their remarkable magnetic and electronic properties. Among them Zn doped Fe_3O_4 nanostructures achieved great interest in clinical applications due to less toxicity and compatibility of Zn^{2+} ion with human body.

However, the reported magnetic properties of $Zn_xFe_{3-x}O_4$ nano materials prepared by different synthesis methods are contradictory. Takaobushi et al. [15,16] reported continuous increase of magnetization (M_s) in $Zn_xFe_{3-x}O_4$ epitaxial thin films till x = 0.9. By contrast, Venkateshvaran et al. [17] observed M_s of $Zn_xFe_{3-x}O_4$ epitaxial films to decrease monotonously with increasing x from 0 to 0.5. Matsuo et al. [18] showed the maximum M_s for x = 0.2 in nanoparticles, prepared by chemical coprecipitation method.

Among all the other nanostructures nano hollow spheres drew maximum attention because of high magnetic saturation, low density, large effective surface area and ability to withstand change in temperature and pressure [19].

In this paper we prepared $Zn_xFe_{3-x}O_4$ ($0.0 \le x \le 1.0$) NHSs to investigate the structural and magnetic properties with Zn doping. M_s increases till x = 0.2 due to replacement of Fe^{3+} by Zn^{2+} in tetrahedral site disturbing the cancellation of magnetic moment of Fe^{3+} in octahedral and tetrahedral sites. This enhanced M_s will enable them for better bio-medical applications.

2. Experimental

$Zn_xFe_{3-x}O_4$ (x = 0.0, 0.1, 0.2, 0.3, 0.4 & 1) NHSs were synthesized using a facile template free solvothermal method through proper variation of Zinc chloride. In the typical synthesis of $Zn_xFe_{3-x}O_4$ NHSs, 1.35 g of $FeCl_3{\cdot}6H_2O$, x g of $ZnCl_2$ ($0 \le x \le 0.291$) and 0.53 g of urea were dissolved in 30 ml solvent mixture of 20 ml Ethylene glycol & 10 ml Ethanol, which were stirred until clear homogeneous solution was obtained. Thereafter, 1 ml of oleylamine which is a growth modifier as well as surface stabilizer was added to the solution mixture in order to restrict the particle growth in nanometer size range. The properly mixed final solution was transferred into 40 ml Teflon lined

* Corresponding author.
E-mail address: priyankasaha@bose.res.in (P. Saha).

https://doi.org/10.1016/j.jmmm.2018.11.061
Received 19 June 2018; Received in revised form 8 November 2018; Accepted 8 November 2018
Available online 09 November 2018
0304-8853/

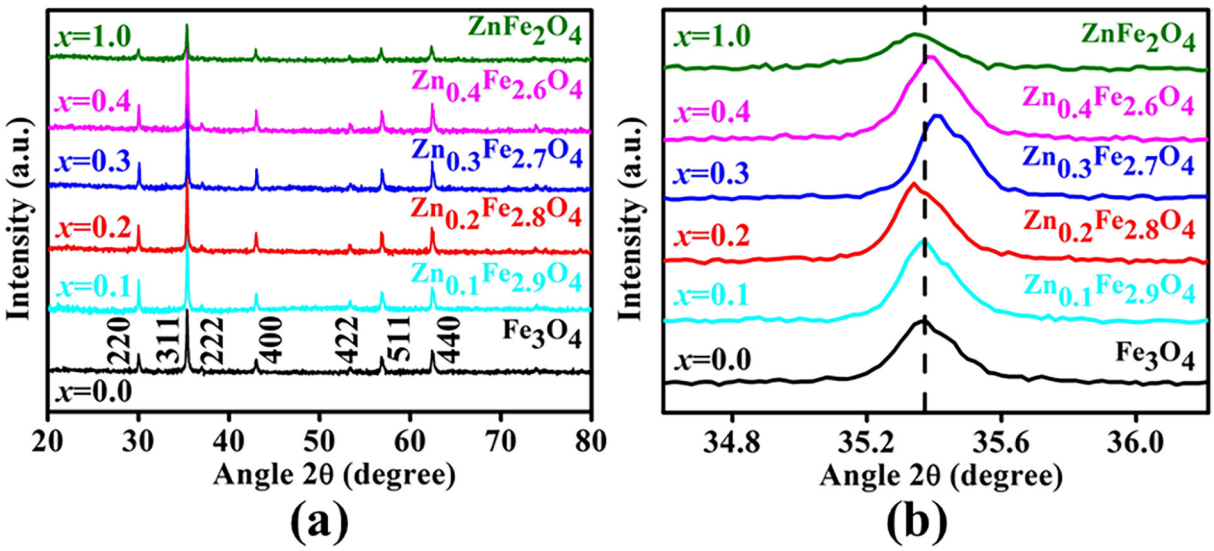

Fig. 1. (a) XRD intensity pattern of $Zn_xFe_{3-x}O_4$ (x = 0.0, 0.1, 0.2, 0.4, 1) with (b) enlarged image of (3 1 1) reflection plane.

Table 1
Values obtained from XRD pattern for different values of Zn concentration.

Sample	Position of (3 1 1) peak in degree (2θ)	Crystallite size (nm)	Lattice Spacing (Å)	Lattice Constant (Å)	Diameter of NHSs From TEM (nm)
Fe_3O_4	35.37	41.56	2.5375	8.4159	130
$Zn_{0.1}Fe_{2.9}O_4$	35.367	41.94	2.5383	8.4186	240
$Zn_{0.2}Fe_{2.8}O_4$	35.337	44.82	2.5402	8.4249	390
$Zn_{0.3}Fe_{2.7}O_4$	35.408	45.04	2.5354	8.4089	310
$Zn_{0.4}Fe_{2.6}O_4$	35.386	49.40	2.5369	8.4139	420
$ZnFe_2O_4$	35.342	37.32	2.5399	8.4239	195

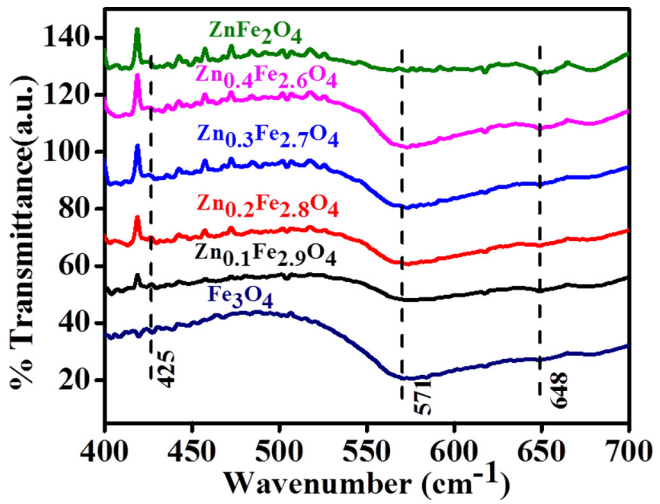

Fig. 2. FTIR spectra of the $Zn_xFe_{3-x}O_4$ NHSs.

stainless steel autoclave and heated to 180 °C for 20 h followed by natural cooling to room temperature. The resulting black precipitate was thoroughly washed with absolute ethanol to remove all residual reagents and separated by centrifugation. The as-obtained product was dried at 60 °C for 12 h. Only by modulating the amount of $ZnCl_2$, we have been able to prepare $Zn_xFe_{3-x}O_4$ (x = 0.0, 0.1, 0.2, 0.4, 1) NHSs. At the elevated temperature urea decomposed to ammonia which produced hydroxyl groups. These hydroxyl groups precipitated the hydroxides of zinc and ferric ions, which finally formed $Zn_xFe_{3-x}O_4$ NHSs.

Phase and morphology of the prepared samples are characterized using X-ray diffraction (XRD) by Rigaku Miniflex II desktop X-ray diffractometer using Cu K_α (λ = 1.5418 Å) radiation, Transmission Electron Microscope (TEM) and Fourier Transform Infrared Spectroscopy (FTIR). The magnetic measurements are performed by Vibrating Sample Magnetometer (VSM) and Superconducting Quantum Interference Device (SQUID).

3. Results and discussions

3.1. Structure and morphology

The XRD patterns of as-prepared $Zn_xFe_{3-x}O_4$ NHSs, as shown in Fig. 1, confirm the formation of face centered cubic spinel structure (JCPDS card np. 89-1397).

We were able to find the variation of lattice constant of $Zn_xFe_{3-x}O_4$ NHSs with the variation of percentage of doping (shown in Table 1), by shifting the Bragg reflection peak (Fig. 1 b) of Miller index (3 1 1). Because of the replacement of Fe^{3+} (0.64 Å) with Zn^{2+} (0.74 Å) in the A site, the distance between the (3 1 1) planes increased, causing higher lattice constant. It is found that up to x = 0.2 the peak shifted towards lower diffraction angle and beyond which the behavior is not consistent. Inconsistency in the result is obtained after x = 0.2 due to the distortion of crystallinity as a result of doping [18].

The FTIR spectrum of the as prepared $Zn_xFe_{3-x}O_4$ (x = 0, 0.1, 0.2, 0.3, 0.4, 1) NHSs shown in Fig. 2 confirms the formation of spinel structure. In the pure Fe_3O_4 NHS (x = 0) spectrum, presence of absorption bands at 571 cm^{-1} wavenumber is due to Fe-O stretching vibrations of Fe^{3+} in tetrahedral sites and those of Fe^{3+} and Fe^{2+} ions at 648 and 425 cm^{-1} in octahedral sites respectively confirm Fe_3O_4 structure formation [20].

Due to conversion of Fe^{2+} ions to Fe^{3+} in octahedral sites and changes in the properties of the created bonds between Fe^{3+} ions and oxygen ions, the absorption bands shift in the FTIR spectra. The shift in the absorption bands is easily observed from Fig. 2.

TEM images of Fe_3O_4 and $ZnFe_2O_4$ NHSs, as shown in Fig. 3(a) and (b), indicate homogeneous size distribution and uniform shape of the samples. The intensive contrast between the dark boundary line and bright center of the TEM images confirm the formation of hollow structure. Hollow structure and uniform shape of the samples are also confirmed from the cracked spheres of FESEM images shown in Fig. 4(a) and (b). Average diameter of the NHSs as mentioned in Table 1

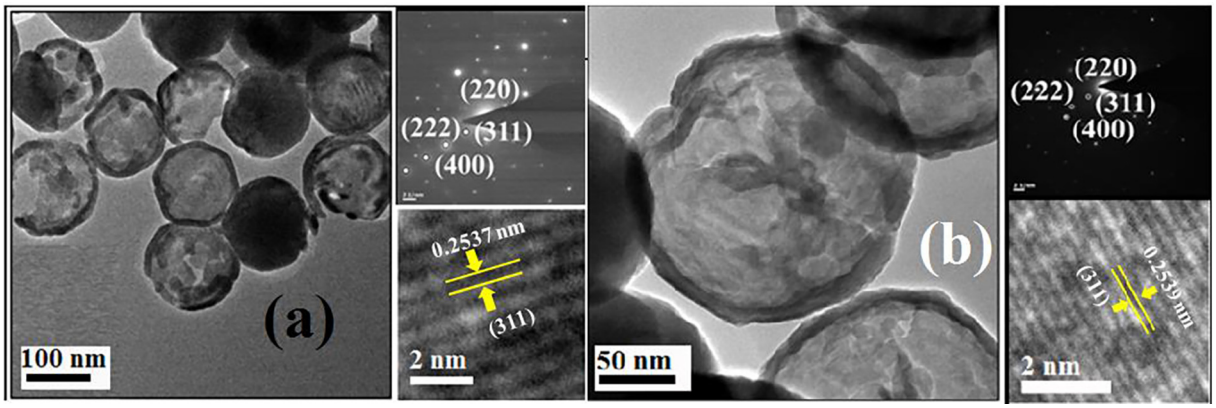

Fig. 3. TEM, HRTEM and SAED pattern of (a) Fe_3O_4 and (b) $ZnFe_2O_4$.

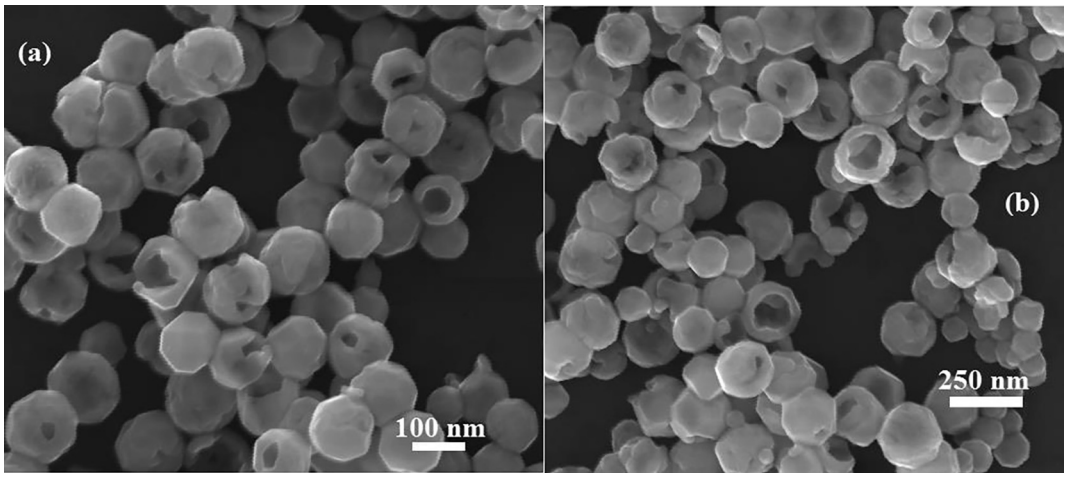

Fig. 4. FESEM images of (a) Fe_3O_4 and (b) $ZnFe_2O_4$.

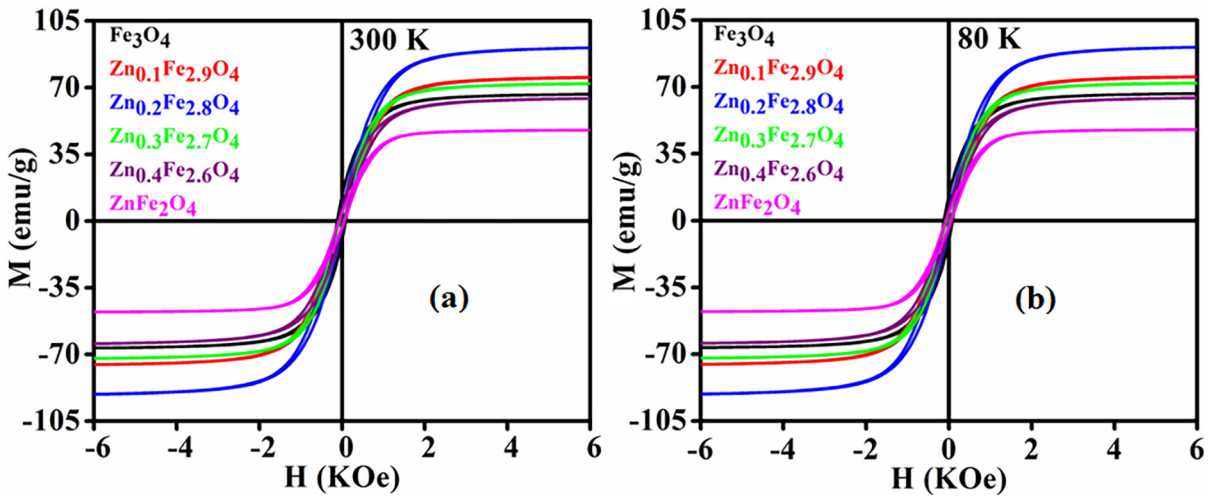

Fig. 5. Variation of Magnetization (M) with applied magnetic field (H) at (a) 300 K and (b) 80 K.

is calculated from TEM and FESEM images. High resolution TEM (HRTEM) and selected area diffraction pattern (SAED) is studied in order to obtain the detailed information about the crystallinity and structure of the as synthesized samples. The HRTEM images as shown in Fig. 3 confirm the crystallinity of the NHSs and the calculated lattice spacing is the same as obtained from the XRD data analysis (Table 1). The information of diffraction plane and lattice constant is obtained from SAED pattern, along with the confirmation of crystallinity, which is in accordance with the data shown in Table 1 from XRD measurement.

3.2. Magnetic measurements

The M-H loop of all the samples at T = 300 K and 80 K is shown in Fig. 5 (a) and (b). We found an increase in the saturation magnetization value (M_s) of the NHSs with Zn doping. Magnetization became

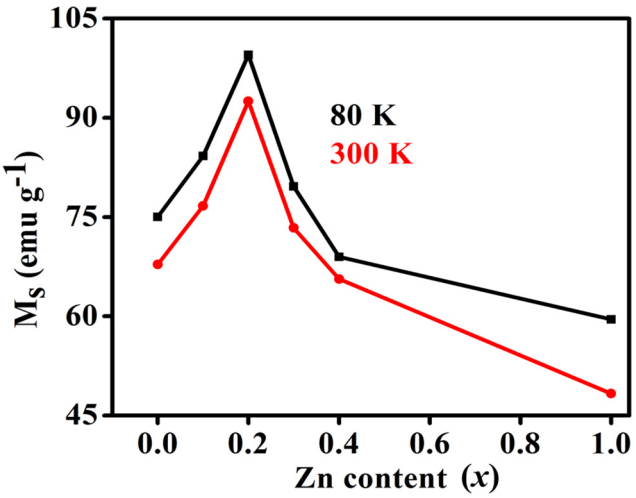

Fig. 6. Variation of Saturation magnetization (M_S) as a function of Zinc content in $Zn_xFe_{3-x}O_4$ at 300 K and 80 K.

maximum for $x = 0.2$ with $M_s = 91.8$ emu-g^{-1} at 300 K and 99.5 emu-g^{-1} at 80 K, which decreased upon further increase in Zinc content.

The magnetic behavior with Zn doping can be explained via exchange interaction [21–23]. The magnetic exchange in magnetite is governed by a combination of antiferromagnetic superexchange (SE) and ferromagnetic double exchange (DE) interactions. The oxygen ions (O_2^-) are arranged to form face centered cubic lattice (FCC) with two kind of sublattices, namely tetrahedral (A-site) and octahedral (B-site) interstitial sites. The A sites (8 per unit cell) are occupied by trivalent Fe_A^{3+} ($3d^5$, S = 5/2), whereas on the octahedrally coordinated B sites (16 per unit cell) there is an alternating arrangement of Fe_B^{2+} ($3d^6$, S = 2) and Fe_B^{3+} ($3d^5$, S = 5/2) ions. Substitution of Fe_A^{3+} by Zn^{2+} reduces the amount of Fe_B^{2+} on the B site to maintain charge neutrality. That is, the amount of itinerant charge carriers mediating the DE interaction on the B sublattice is reduced [17]. This reduction in ferromagnetic DE interaction and strengthening in antiferromagnetic SE interaction introduce Yafet-Kittel angle [24], reducing the saturation magnetization after certain doping concentration.

From the temperature dependent magnetic hysteresis loops we found that the M_s value to be gradually increasing with decreasing temperature for all samples, where the value of coercivity and remanence showed an increase. The small increase in coercivity at lower temperature is due to reduction in thermal fluctuation. Fig. 6 shows the variation of M_s with zinc content (x) at room temperature and at 80 K. Saturation magnetization increases at lower temperature due to decrease in thermal energy, so that the magnetic moment got aligned along the field direction easily [25]. On the other hand due to thermal fluctuation and other disorder states at the surface of the NHSs the response of magnetic moment with magnetic field is weak at higher temperature.

The Zero field cooled (ZFC) and field cooled (FC) χ vs T measurements are shown in Fig. 7 for $Zn_xFe_{3-x}O_4$ NHSs with an applied field of 100 Oe. The observed cusp-like maxima in the ZFC-FC curves correspond to the spin glass transition mainly from the surface spins. Magnetization in a nanoparticle is contributed from the inner part where strong magnetic ordering exists and from the surface part where magnetic order is not so strong. Higher magnetization of the FC curve compared to corresponding ZFC curve is attributed to the surface spins, which are frozen in the external field direction. Even the ZFC curves show high magnetization at the lowest temperature (3 K) due to the contribution from the inner part. Another cusp like maxima observed at the higher temperature region corresponds to Verwey transition where structural transition of magnetite samples from cubic to monoclinic symmetry takes place on decreasing temperature. Verwey transition is absent in $ZnFe_2O_4$.

AC susceptibility measurements are important as the dependence of susceptibility on temperature T is useful in detecting variations in magnetic anisotropy. The real (χ') and imaginary (χ'') parts of AC susceptibility, for $x = 0.0$, $x = 0.2$ and $x = 1.0$, are shown in Fig. 8 at four different frequencies $f = 7$ Hz, 83 Hz, 253 Hz & 503 Hz and in the temperature range 5 K to 400 K. We observed two peaks in the susceptibility vs temperature curves, lower temperature peak (T_1' for χ' and T_1'' for χ'') corresponds to the spin freezing temperature and higher temperature peak (T_2' for χ' and T_2'' for χ'') indicates the Verwey transition. With frequency χ'' changes significantly due to the presence of dipolar interactions between NHSs.

Frequency dependence of χ' for $T < T_1'$ and its frequency independence for $T > T_1'$, suggests the frequency dependence transition of the NHSs. Variation of T_1' and T_1'' with frequency is related to the

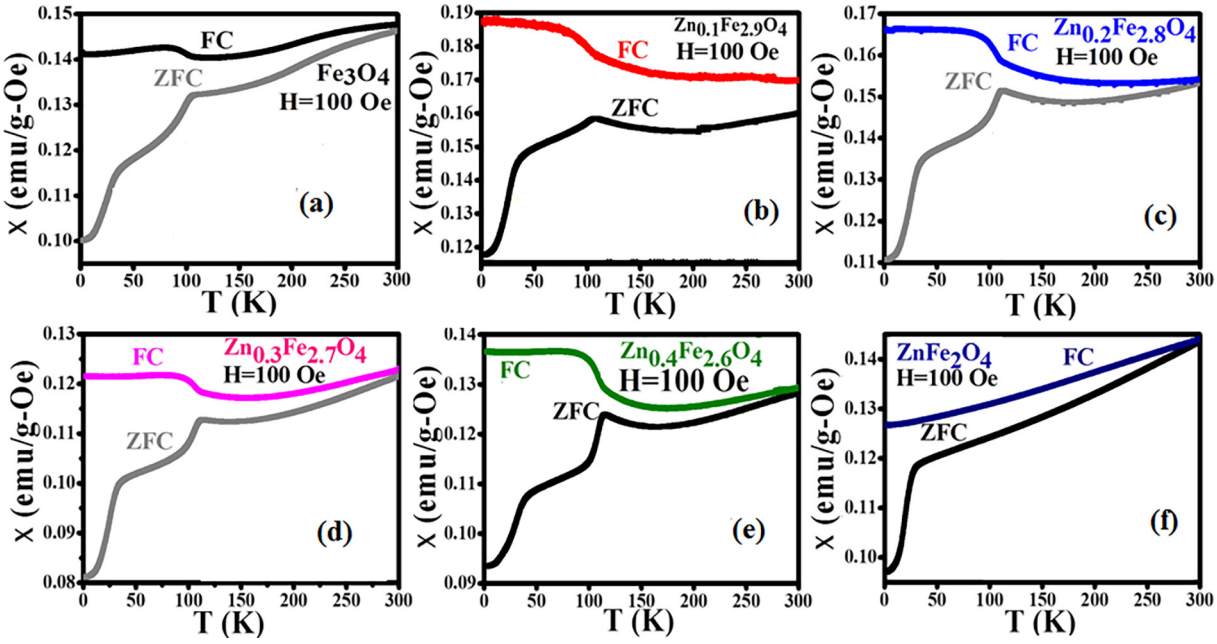

Fig. 7. ZFC-FC curves of the $Zn_xFe_{3-x}O_4$ NHSs.

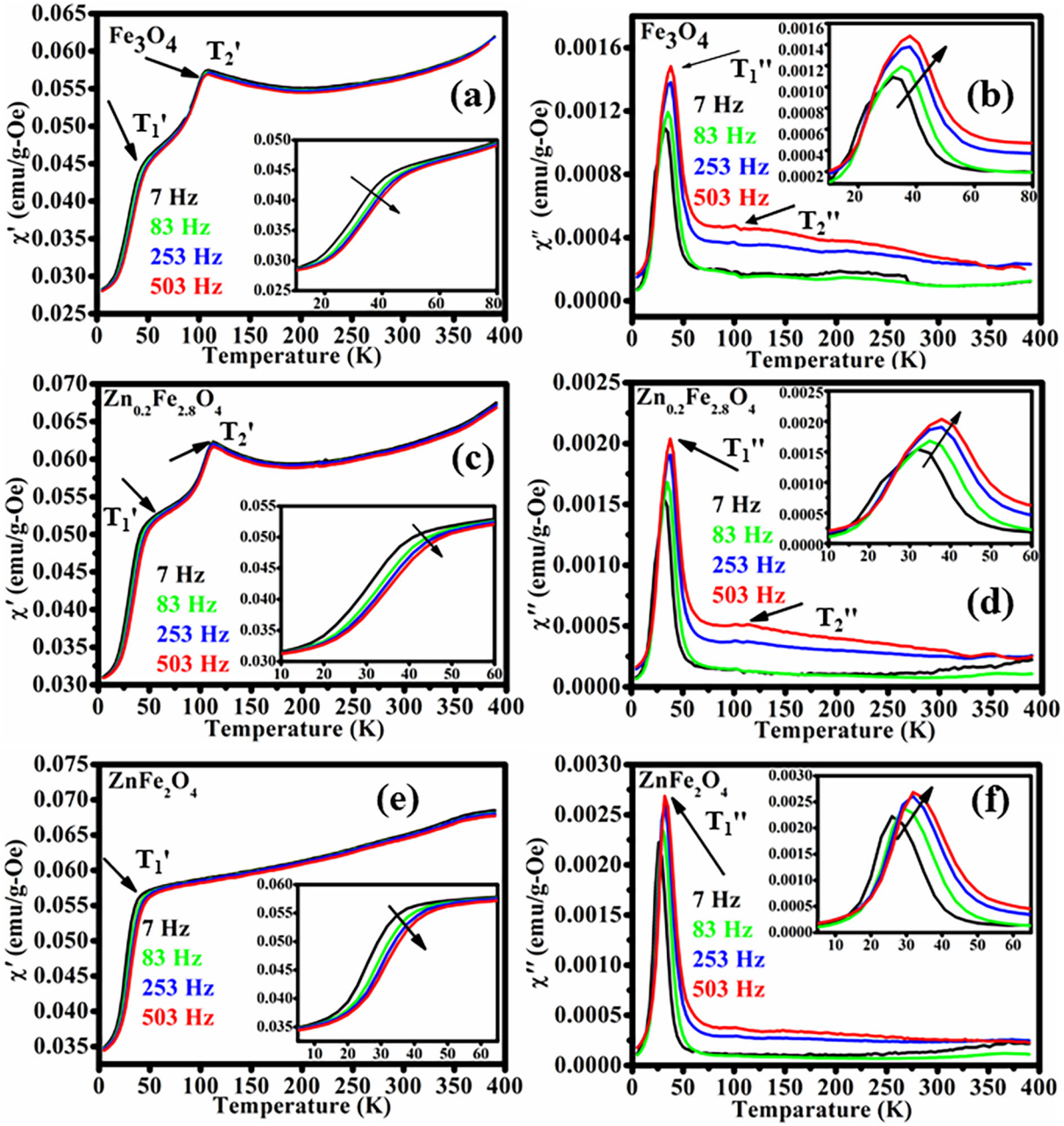

Fig. 8. Temperature dependent susceptibility curves of (a-b) Fe_3O_4, (c–d) $Zn_{0.2}Fe_{2.8}O_4$, (e-f) $ZnFe_2O_4$.

relaxation of domain walls [26], which resulted in higher magnetic anisotropy as well as spin freezing temperature. For better understanding of the low temperature magnetic behaviour, peak shift of χ' with frequency can be considered by analysing [27]

$$\Gamma = \frac{\Delta T_1'}{T_1' \Delta \log f} \tag{1}$$

The values of Γ obtained for x = 0.0, 0.2 and 1.0 are 0.033, 0.038 and 0.05 respectively, which clearly indicate the spin glass type behaviour as $\Gamma < 0.06$ [27]. Moreover from Fig. 8 it is clear that χ' depends strongly on frequency around 40 K, whereas in χ'' the peak shifts towards higher temperature with increasing frequency. This behaviour suggests a high temperature ferromagnetic to low temperature spin glass magnetic state at the surface [28,29].

In order to get clear sight into the relaxation mechanism of the nano hollow spheres we fit the data of relaxation time and T_1' with Vogel-Fulcher equation [26]:

$$\tau = \tau_0 \exp[-E_a/k_B(T_1' - T_0)] \tag{2}$$

Where, E_a is the anisotropy energy barrier, τ_0 is the characteristic relaxation time, k_B is the Boltzmann constant and T_0 is the characteristic temperature which is the measure of the interaparticle interaction energy.

By fitting with Eq. (2) (Fig. 9) we found $\tau_0 = 1.14 \times 10^{-8}$ s and $T_0 = 41.0 \pm 0.2$ K for $x = 0$ for $E_a/k_B = 189$ K. This type of large τ_0 is expected for interacting spin cluster [30]. For $x = 0.2$ and 1.0 the values of τ_0 and T_0 are 2.56×10^{-9} s and 36.0 ± 0.5 K for $E_a/k_B = 276$ K and 1.53×10^{-8} s and 25 ± 0.6 K for $E_a/k_B = 219$ K respectively. Interparticle interaction energy decreases with increasing Zn doping, indicating reduced magnetic dipole-dipole interaction.

Verwey transition temperature T_2' or T_2'', where cubic to monoclinic structural transition takes place, depends on the transition metals present in the compound [31]. Verwey transition is independent of frequency [32] and weakly size dependent [33]. It is extremely

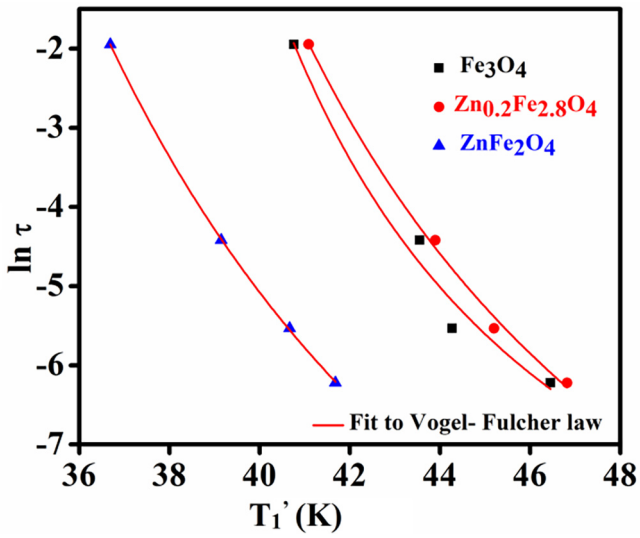

Fig. 9. Frequency dependence of T_1' fitted to Vogel- Fulcher Law.

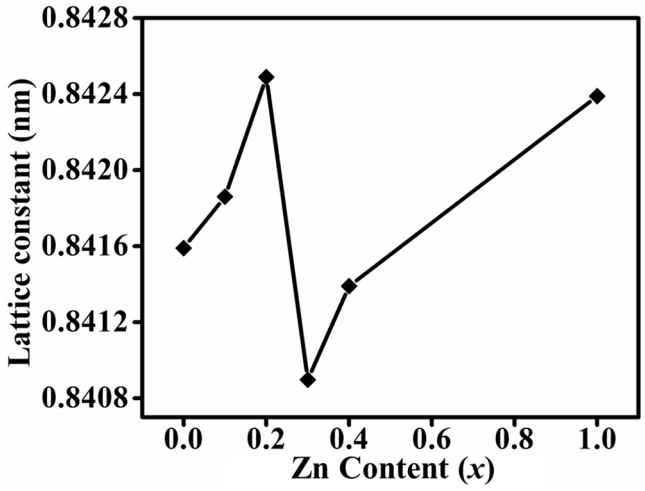

Fig. 10. Variation of lattice parameter with Zn content (x).

Table 2
Verwey transition temperature of $Zn_xFe_{3-x}O_4$ NHSs.

$Zn_xFe_{3-x}O_4$	T_V' (K)	T_V'' (K)
Fe_3O_4	108.03	103.6
$Zn_{0.1}Fe_{2.9}O_4$	109.8	106.82
$Zn_{0.2}Fe_{2.8}O_4$	112.68	112.82
$Zn_{0.3}Fe_{2.7}O_4$	112.5	112.5
$Zn_{0.4}Fe_{2.6}O_4$	115.4	115.3

sensitive to the Oxygen Stoichiometry. Gupta et al. [31] has shown that there is a role of phonon in determining the Verwey transition temperature. Since Zn^{2+} replaces Fe^{3+} at the A sites around which the vibrating oxygen ions are situated, the changes in frequency of phonon vibration (ν) is expected. ν can be written as [31]

$$\nu = \frac{1}{2\pi}\sqrt{\frac{k}{m_r}} \tag{3}$$

where, the reduced mass $m_r = \frac{m_1 m_2}{m_1 + m_2}$ and k is bond strength.

Here, m_1 = mass of Zn^{+2}/mass of Fe^{+3} and m_2 = mass of O^{-2}. From Eq. (3), ν increases with increasing k and decreasing m_r. Verwey transition temperature decreases with increasing frequency of phonon vibration as reported earlier [31]. With increasing Zn^{2+} (65.408 Dalton) doping, replacing Fe^{+3} (55.843 Dalton), reduced mass increases as $m_{0.2} < m_{0.3} < m_{0.4}$, hence as a result ν should decrease as $\nu_{0.2} > \nu_{0.3} > \nu_{0.4}$.

On the other hand, as ionic radius of Zn^{2+} (0.74 Å) is higher than that of Fe^{3+} (0.64 Å) lattice constant increases reducing the bond strength k, which therefore reduces the frequency of phonon vibration (ν). In our case we have seen that $a_{0.2} > a_{0.4} > a_{0.3}$ (Fig. 10). Due to the combined effect of mass and bond strength, we obtain an average effect, $T_{v0.4} > T_{v0.2} > T_{v0.3}$ (Table 2)

4. Conclusion

The structural and magnetic properties of $Zn_xFe_{3-x}O_4$ NHSs are investigated to observe an increase in magnetic moment from 65.49 emu/g for $x = 0.0$ to 92.5 emu/g for $x = 0.2$, beyond which it reduces due to spin canting. The temperature and frequency dependent dynamic magnetization study revealed the reduction in interparticle interaction energy with increasing Zn doping due to reduced magnetic dipolar interaction. $Zn_xFe_{3-x}O_4$ NHSs with improved magnetism is a promising material for bio-medical applications.

Acknowledgement

This work is acknowledged to the Department of Science and Technology (INSPIRE), Government of India for financial support. Funding from SNBNCBS is also gratefully acknowledged.

Appendix A. Supplementary data

Supplementary data to this article can be found online at https://doi.org/10.1016/j.jmmm.2018.11.061.

References

[1] S.W. Cao, Y.J. Zhu, M.Y. Ma, L. Li, L. Zhang, J. Phys. Chem. C. 112 (2008) 1851–1856.
[2] F.Q. Hu, L. Wei, Z. Zhou, Y.L. Ran, Z. Li, M.Y. Gao, Adv. Mater. 18 (2006) 2553–2556.
[3] Catherine C. Berry, Adam S.G. Curtis, J. Phys. D: Appl. Phys. 36 (2003) R198–R206.
[4] F.Y. Cheng, C.H. Su, Y.S. Yang, C.S. Yeh, C.Y. Tsai, C.L. Wu, M.T. Wu, D.B. Shieh, Biomaterials 26 (2005) 729–738.
[5] C. Yao, Q. Zeng, G.F. Goya, T. Torres, J. Liu, H. Wu, M. Ge, Y. Zeng, Y. Wang, J.Z. Jiang, J. Phys. Chem. C 111 (2007) 12274–12278.
[6] G.V.M. Jacintho, A.G. Brolo, P. Corio, P.A.Z. Suarez, J.C. Rubim, J. Phys. Chem. C. 113 (2009) 7684–7691.
[7] Q. He, H.Z. Wang, G.H. Wen, Y. Sun, B. Yao, J. Alloys Compd. 486 (2009) 246–249.
[8] L. Li, G. Li, R.L. Smith, H. Inomata, Chem. Mater. 12 (2000) 3705–3714.
[9] M. Mozaffari, S. Manouchehri, M.H. Yousefi, J. Amighian, J. Magn. Magn. Mater. 322 (2010) 383–388.
[10] Y. Zhuo, P.X. Yuan, R. Yuan, Y.Q. Chai, C.L. Hong, Biomaterials 30 (2009) 2284–2290.
[11] L. Luo, L. Zhu, Y. Xu, L. Shen, X. Wang, Y. Ding, Q. Li, D. Deng, Microchim. Acta. 174 (2011) 55–61.
[12] P. Kalita, J. Singh, M.K. Singh, P.R. Solanki, G. Sumana, B.D. Malhotra, Appl. Phys. Lett. 100 (2012) 093702.
[13] A. Kaushik, R. Khan, P.R. Solanki, P. Pandey, J. Alam, S. Ahmad, B.D. Malhotra, Biosens. Bioelectron. 24 (2008) 676–683.
[14] A. Go¨imez-Hens, J.M. Fernaǐndez-Romero, M.P. Aguilar-Caballos, Trends Anal. Chem. 27 (2008) 394–406.
[15] J. Takaobushi, M. Ishikawa, S. Ueda, E. Ikenaga, J.J. Kim, M. Kobata, Y. Takeda, Y. Saitoh, M. Yabashi, Y. Nishino, D. Miwa, K. Tamasaku, T. Ishikawa, I. Satoh, H. Tanaka, K. Kobayashi, T. Kawai, Phys. Rev. B. 76 (2007) 205108.
[16] J. Takaobushi, H. Tanaka, T. Kawai, S. Ueda, J. Kim, M. Kobata, E. Ikenaga, M. Yabashi, K. Kobayashi, Y. Nishino, D. Miwa, K. Tamasaku, T. Ishikawa, Appl. Phys. Lett. 89 (2006) 242507.
[17] D. Venkateshvaran, M. Althammer, A. Nielsen, S. Geprägs, M.S. Ramachandra Rao, S.T.B. Goennenwein, M. Opel, R. Gross, Phys. Rev. B 79 (2009) 134405.
[18] J. Liu, Y. Bin, M. Matsuo, J. Phys. Chem. C. 116 (2012) 134–143.
[19] F. Wang, J. Liu, J. Kong, Z.X. Wang, M. Itoh, K.I. Machida, J. Mater. Chem. 21 (2011) 4314–4320.
[20] Z.R. Marand, M.H.R. Farimani, N. Shahtahmasebi, Nanomed J. 1 (2014) 238–247.
[21] J. Loos, P. Novak, Phys. Rev. B. 66 (2002) 132403.
[22] R.J. McQueeney, M. Yethiraj, S. Chang, W. Montfrooij, T.G. Perring, J.M. Honig, P. Metcalf, Phys. Rev. Lett. 99 (2007) 246401.
[23] A. Rosencwaig, Phys. Rev. 181 (1969) 946.

[24] Y. Yafet, C. Kittel, Phys. Rev. 87 (1952) 290.
[25] C. Caizer, M. Stefanescu, J. Phys. D: Appl. Phys. 35 (2002) 3035–3040.
[26] J.L. Tholence, Solid State Commun. 35 (1980) 113–117.
[27] J.A. Mydosh, Spin Glasses: An Experimental Introduction, Taylor and Francis, London, 1993.
[28] B.R. Coles, B.V.B. Sarkissian, R.H. Taylor, Philos. Magn. B 37 (1978) 489.
[29] E. Bonetti, L. Del Bianco, D. Fiorani, D. Rinaldi, R. Caciuffo, A. Hernando, Phys. ReV. Lett. 83 (1999) 2829.
[30] B. Idzikowski, U.K. Rößler, D. Eckert, K. Nenkov, K. Dörr, K.H. Müller, Euro phys. Lett. 45 (1999) 714.
[31] R. Gupta, A.K. Sood, P. Metcalf, J.M. Honig, Phys. Rev. ew B 65 (2002) 104430.
[32] D.A. Clark, P.W. Schmidt, Phys. Earth Planet. Inter. 30 (1982) 300–316.
[33] J. Lee, S.G. Kwon, J.G. Park, T. Hyeon, Nano Lett. 15 (2015) 4337–4342.